eLife

Reviewed Preprint
v1 • August 13, 2026
Not revised

For correspondence:
peng@fudan.edu.cn
yanxiarao@fudan.edu.cn

Author notes: See page 17

Funding: See page 17

Reviewing editor: Florent Ginhoux, Singapore Immunology Network, Singapore

Lineage tracing and live-cell imaging reveal that NeuroD1 does not reprogram microglia into neurons

Xiaoyu Li[1,2,#], Yuxin Li[1,#], Yue Cao[1,2,#], Niewen Hu[1,2], Baozhi Yang[2], Pei Ouyang[1,2], Yuxiao Jin[2], Shuai Gao[1,2], Bo Peng[1,3] ✉, Yanxia Rao[1,2] ✉

[1]National Children's Medical Center, Children's Hospital, Institute for Translational Brain Research, State Key Laboratory of Medical Neurobiology, MOE Frontiers Center for Brain Science, MOE Innovative Center for New Drug Development of Immune Inflammatory Diseases, Shanghai Key Laboratory of Gene Editing and Cell Therapy for Rare Diseases, Fudan University, Shanghai, China • [2]Department of Neurology, Zhongshan Hospital, Laboratory Animal Center, MOE Frontiers Center for Brain Science, Fudan University, Shanghai, China • [3]Department of Neurosurgery, Huashan Hospital, Fudan University, Shanghai, China

eLife Assessment

This is a **valuable** study addressing a debated question in brain repair research by testing whether NeuroD1 can convert brain immune cells into nerve cells using a virus-free genetic approach and live imaging. The **solid** evidence presented here supports that, under the conditions tested, NeuroD1-expressing cells do not become nerve cells and instead retain their original identity; however, some aspects of expression level, injury timing, and cell-type composition would benefit from further clarification. This work will be of interest to neuro-immunologists.

https://doi.org/10.7554/eLife.112083.1.sa2

Abstract

Induction of glia-to-neuron conversion is a promising regenerative strategy for treating brain injuries and neurodegenerative diseases. Previous studies have suggested that NeuroD1 can induce microglia-to-neuron cross-lineage conversion. However, it remains highly controversial. To conclusively determine whether NeuroD1 can convert microglia into neurons, we used genetic fate mapping to track the cell fate of microglia ectopically expressing NeuroD1. Furthermore, we performed two-photon imaging to trace the fate of the NeuroD1-expressing microglia. Our findings revealed that cells ectopically expressing NeuroD1 are bona fide microglia, not neurons, regardless of injury preconditioning. Additionally, NeuroD1 overexpression in microglia did not promote brain injury recovery, and the microglial identity remained intact. These results provide solid evidence that NeuroD1 cannot convert microglia into neurons. Our study underscores the necessity of lineage-tracing and cell fate mapping strategies to verify glia-to-neuron conversion, highlighting the importance of rigorous validation in regenerative research.

Introduction

Neurons in the central nervous system (CNS) possess limited regenerative capacity, resulting in permanent neuronal loss after injury or damage. In contrast, glia especially microglia exhibit a higher regenerative capacity(1–3). Reprogramming glial cells with regenerative potential into neurons lacking regenerative capacity offers a promising strategy for repairing damage in the CNS. The glia-to-neuron conversion process is achieved primarily by the overexpression of specific fate-determining factors or the knockdown of certain genes. The manipulation of single genes such as NeuroD1 (4), PAX6 (5), SOX2 (6–9), ASCL1 (10) and PTBP1 (11, 12) has been reported to induce inter-neuroectodermal lineage conversion, transforming astrocytes, oligodendrocyte precursor

cells (OPCs) or Muller glia into neurons. While this approach may hold significant potential for clinical therapies, it still requires validation through more stringent and robust approaches. Well-controlled lineage tracing and unambiguous live imaging are gold standards for demonstrating the glia-to-neuron conversion (13, 14). However, controversial studies employing rigorous lineage tracing and live imaging techniques have failed to observe some inter-lineage glia-to-neuron conversions under single-gene manipulation (15–23), including NeuroD1 (21–23). In addition to inter-lineage conversion, Nakashima et al. have reported a NeuroD1-induced microglia-to-neuron cross-lineage conversion (24). Using lentiviral overexpression of NeuroD1, we conducted lineage tracing, *in vitro* live-cell imaging, and microglia ablation, demonstrating that the previously reported cross-lineage conversion of microglia into neurons is a result of experimental artifacts, e.g., off-target transduction from virus (13). Although Nakashima et al. argued that the phenomenon we observed was due to insufficient NeuroD1 expression in microglia (25), our comparison of the data from both studies (13, 24) indicates that our NeuroD1 expression levels are comparable to, or even higher than, those reported in their study (26).

Surprisingly, Nakashima et al. recently reported that NeuroD1 can not only can achieve the cross-lineage conversion of microglia into neurons at brain injury sites *in vivo*, but also promotes recovery from brain injury (27). The implementation of novel yet contentious strategies in clinical trials or practice requires extreme caution. Such conflicting reports are of particular concern because they directly influence the potential translation of glia-to-neuron reprogramming strategies into therapeutic applications. To address this controversy, we have employed a comprehensive combination of methodologies, including genetic lineage tracing (virus-independent to prevent potential leakage) and two-photon *in vivo* live imaging (enabling direct observation of NeuroD1-expressing microglial cell fate). Our findings unequivocally demonstrate that microglia do not undergo conversion into neurons *in vivo* under either physiological or pathological conditions. These results underscore the critical importance of employing rigorous lineage tracing and cell fate mapping techniques to validate glial reprogramming approaches.

Results

Microglia-specific NeuroD1 expression using a virus-free genetic lineage tracing system

In our previous study, lineage tracing revealed that lentivirus-driven ectopic expression of NeuroD1 does not induce the conversion of microglia into neurons but rather triggers microglial cell death through BCL2-dependent apoptosis (28). However, the viral tools used demonstrated limited efficiency in specifically targeting microglia *in vivo* and resulted in off-target neuronal expression, regardless of whether lentivirus or adeno-associated virus (AAV) (with different serotypes 6, 8 and 9) was employed, and irrespective of the use of CX3CR1 or CD68 promoters (Figure S1). Similar observations have also been reported by our prior study and those of other groups (21, 28, 29).

Direct evidence for glia-to-neuron conversion by NeuroD1 via a virus-free ectopic expression system genetic lineage tracing is lacking, by which avoids experimental artifacts from virus leakage. Thus, we utilized transgenic animals to ectopically express NeuroD1 in microglia and track the cell fate of microglia expressing NeuroD1. We crossed a microglia-specific mouse line CX3CR1-CreER (30) with an inducible NeuroD1-expressing mouse line Rosa26-LoxP-Stop-LoxP-NeuroD1-IRES-GFP (LSL-NeuroD1-GFP) (31), to obtain CX3CR1-CreER::LSL-NeuroD1-GFP mice(NeuroD1^{MG} for short). After tamoxifen treatment, NeuroD1 was ectopically expressed in microglia, accompanied by GFP for lineage tracing (Figure 1A). After tamoxifen administration, the majority of GFP^{+} cells faithfully express NeuroD1 in both the cortex and the striatum across time (Figure 1B-D, Figure S2). Results showed that GFP was specifically expressed in microglia avoiding off-target expression in neurons (Figure 1E-H).

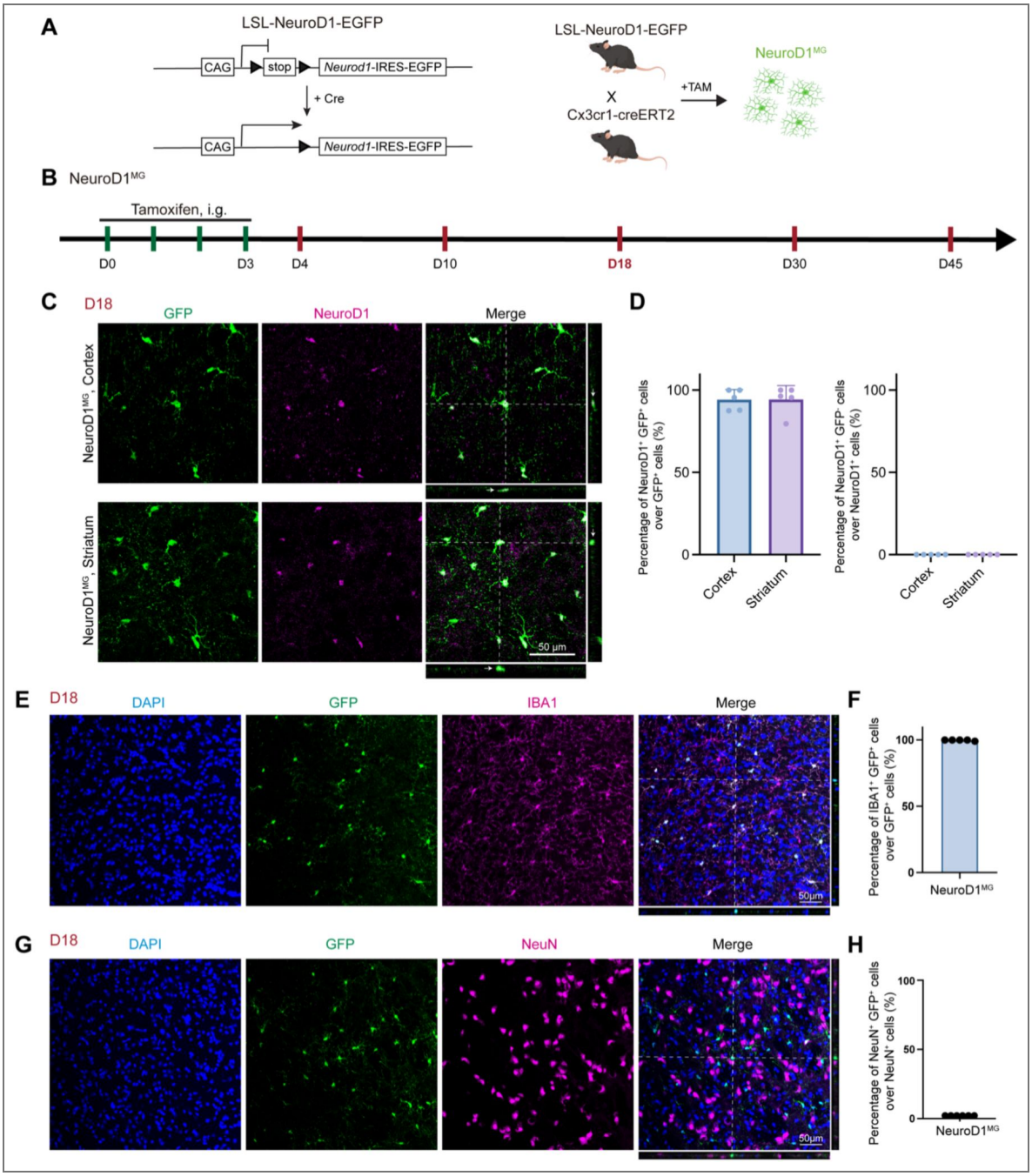

Figure 1. Genetic gain of function of NeuroD1 does not result in microglia-to-neuron conversion in the adult mouse brain.

(A) Schematic of the specific expression of NeuroD1 and lineage tracing of microglia. (B) Experimental timeline. (C) Representative confocal images at D18 showing that NeuroD1 is robustly co-expressed in GFP-positive cells after Cre recombination. (D) Quantification of the percentage of NeuroD1$^+$GFP$^+$ cells among GFP$^+$ cells and NeuroD1$^+$GFP$^-$ cells among NeuroD1$^+$ at D18, revealing NeuroD1 is highly co-expressed with GFP. N = 5 mice for each group. (E) Representative confocal images at D18 showing that GFP-positive cells do not colocalize with neuronal marker NeuN. (F) Quantification of NEUN$^+$GFP$^+$ double-positive cells in NEUN$^+$ cells at D18. N = 6 mice for each group. (G) Representative confocal images at D18 showing that GFP-positive cells do colocalize with microglial marker IBA1. (H) Quantification of IBA1$^+$GFP$^+$ double-positive cells in GFP$^+$ cells at D18. N = 5 mice for each group. Data are presented as mean ± SD.

NeuroD1 fails to induce microglia-to-neuron conversion *in vivo*

Based on this stringent lineage tracing tool, all GFP$^+$ cells remained IBA1$^+$ microglia across all examined time points (4, 10, 18, 30, and 45 days post–tamoxifen induction; Figure 1E, F, Figure 2B,D). Consistently, no GFP$^+$NeuN$^+$ double-positive cells were detected, indicating that ectopic expression of NeuroD1 did not induce microglia-to-neuron conversion (Figure 1G,H, Figure 2B,D). Besides, GFP$^+$ cells were also not co-labeled with MAP2 or TUJ1(Figure S3). Therefore, the genetic lineage tracing experiment reveals that NeuroD1 cannot drive microglia-to-neuron conversion *in vivo*.

NeuroD1 expression induces microglial loss but not conversion *in vivo*

Since immunostaining might yield false-positive signals in the absence of true expression, we further examined microglial states *in vivo* using 2-photon microscopy to track NeuroD1-expressing, GFP-labeled microglia. Imaging of GFP$^+$ cells in the cortex of NeuroD1^{MG} mice was performed every 4 days starting from 18 days post–tamoxifen induction (Figure 3A). Through 2-photon imaging, we did not observe any morphological evidence of microglia-to-neuron conversion. Instead, the GFP-expressing cells exhibited highly ramified morphologies with long processes characteristic of microglia, rather than typical morphology of neuronal cells (Figure 3B, Movie 1). Notably, some GFP-labeled microglia disappeared over time(Figure 3B, yellow arrow), suggesting that NeuroD1 expression does not induce microglia to neuron conversion but instead promotes microglial cell death *in vivo*, consistent with our previous *in vitro* findings(32).To further assess this effect, we quantified GFP$^+$ microglia over time after tamoxifen induction. The number of GFP$^+$ cells initially increased and peaked at D30, but subsequently declined by D45 (Figure 3C, D), supporting the conclusion that NeuroD1 expression contribute to microglia loss *in vivo*. To further investigate the mechanisms underlying microglial loss following NeuroD1 overexpression, we examined markers of autophagy in cortical sections at D18. In NeuroD1^{MG} mice, reporter$^+$ cells exhibited about 4-fold higher LC3 and P62 levels than controls, as shown by immunostaining (Figure 3E-G), indicating accumulation of autophagosomal markers and suggesting impaired autophagic flux. Consistent with increased cell death, TUNEL staining revealed the increase of TUNEL+ cells among reporter$^+$ cells in NeuroD1^{MG} mice relative to controls (Figure S4). Taken together, these data indicate that NeuroD1 overexpression triggers cellular stress and death pathways (including autophagy dysfunction and apoptosis), leading to microglial loss in vivo rather than microglia-to-neuron conversion.

NeuroD1 fails to reprogram microglia into neurons even after traumatic brain injury

Previous studies have suggested that injury-induced environments might facilitate glial cell fate reprogramming. For example, Heinrich et al. demonstrated that a stab wound prior to virus delivery is required for SOX2-mediated conversion of NG2 glia(33). Irie et al. showed that NeuroD1 can directly reprogram microglia/macrophages into neurons at the lesion site following transient middle cerebral artery occlusion(27). Likewise, Chen et al. reported that NeuroD1 converts astrocytes into neuron after spinal cord injury (SCI). These findings suggest that the failure of NeuroD1-mediated microglia-to-neuron conversion under physiological conditions may result from an unfavorable microenvironment.

To test the possibility, we subjected *NeuroD1*^{MG} mice to traumatic brain injury (TBI) in the motor cortex, followed by tamoxifen induction, and utilized Cx3cr1-creER::Ai14 (Ai14^{MG}) mice as controls (Figure 4A). Firstly, we performed grip strength task and rotarod tests to evaluate whether NeuroD1 expression in microglia could ameliorate motor deficits in TBI (Figure 4A). In grip strength task, the NeuroD1-overexpression group showed comparable performance to controls, with no significant differences in the strength across groups (Figure 4B). Similarly, no improvements were observed in rotarod task, reflected by the latency to fall (Figure 4C), indicating that NeuroD1 expression in microglia does not rescue TBI-induced motor dysfunction.

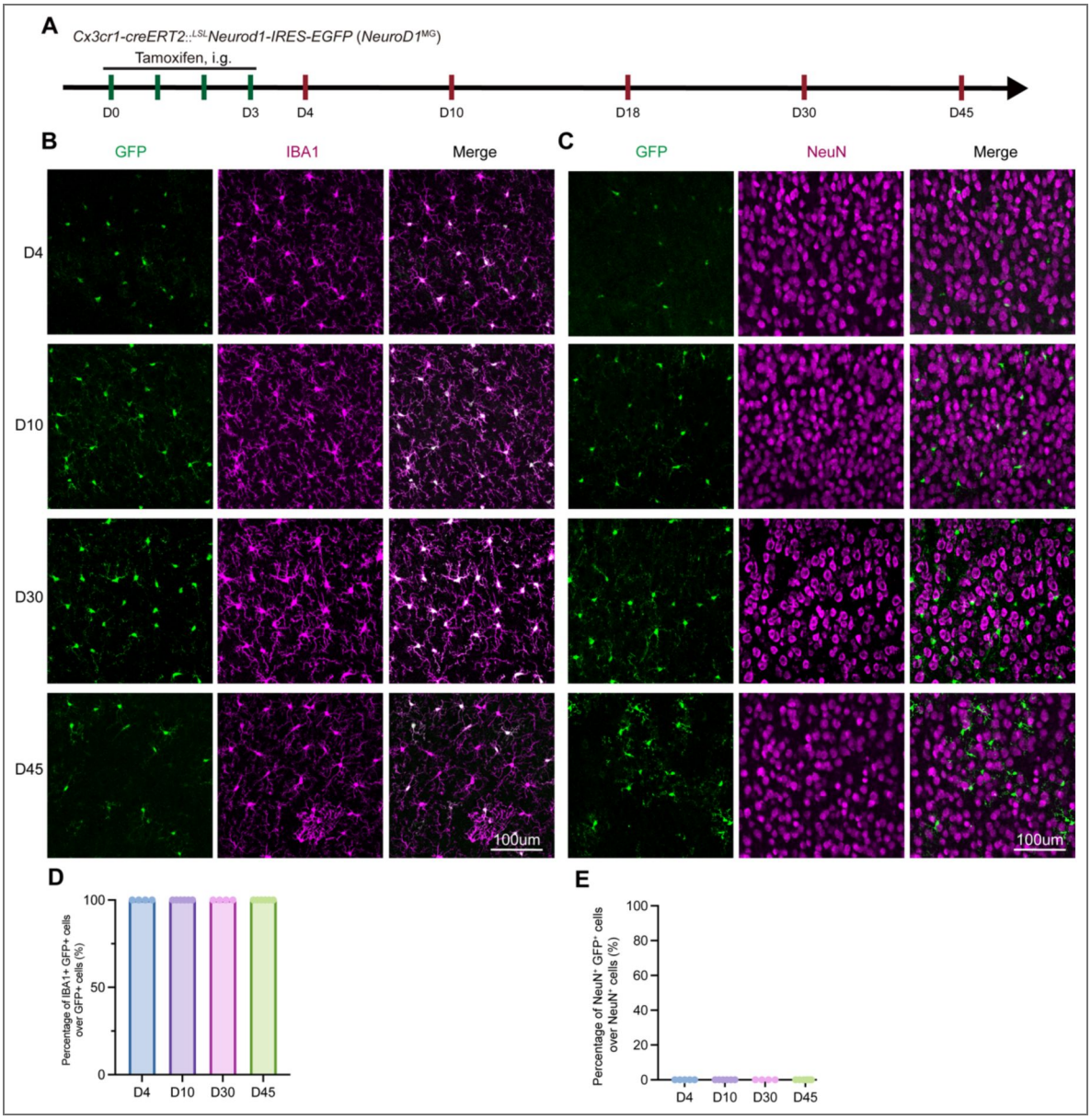

Figure 2. Ectopic NeuroD1 expression in microglia does not induce microglia-to-neuron conversion across time.

(A) Experimental timeline. (B) Representative confocal images at D4, D10, D30 and D45 showing that GFP is co-labeled with IBA1. (C) Representative confocal images at D4, D10, D30 and D45 showing that GFP is not co-labeled with NeuN. (D) Quantification of $IBA1^+GFP^+$ double-positive cells among GFP^+ cells at D4, D10, D30 and D45. N = 4 or 5 mice for each group. (D) Quantification of $NeuN^+GFP^+$ double-positive cells among GFP^+ cells at D4, D10, D30 and D45. N = 4 or 5 mice for each group.

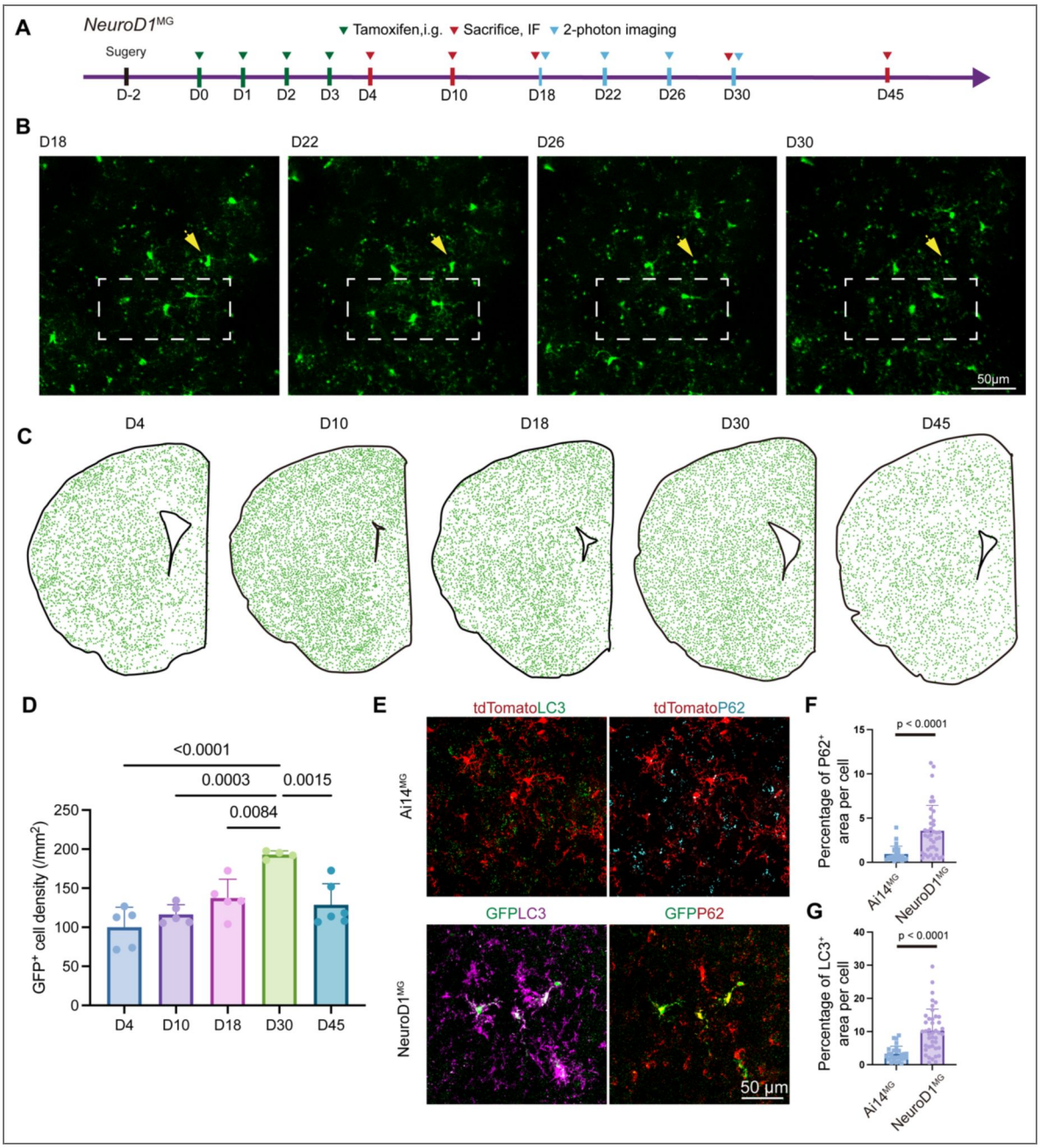

Figure 3. NeuroD1-expressing microglia retain microglial morphology and decline in number over time.

(A) Experimental timeline. (B) Representative images showing GFP-positive cells with highly ramified morphologies characteristic of microglia rather than neurons. (C) Represent images illutrating changes in the number of GFP-postive cells over time (green dots indicate GFP-positive cell). (D) Quantification of GFP-positive cells density.N = 4 - 6 mice per time point. Data are presented as mean ± SD. One Way ANOVA with Turkey's multiple comparison test. (E) Represent confocal image shows the LC3 and P62 level in control and NeuroD1MG mice. Scale bar = 50μm. (F) Quantification of $P62^{+}$ area per cell. Unpaired t test. (G) Quantification of $LC3^{+}$ area per cell. Unpaired t test. (H) Data are presented as mean ± SD.

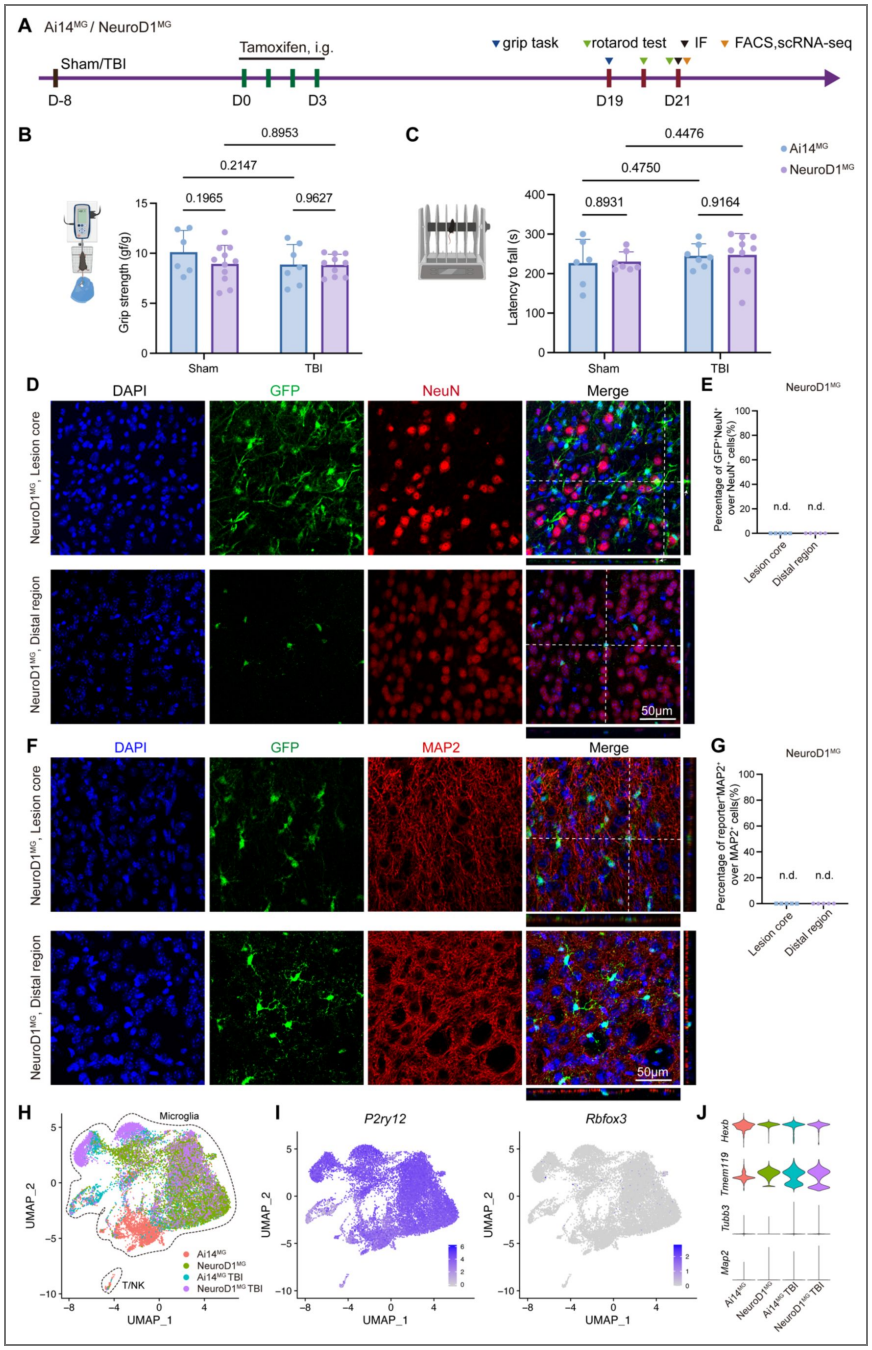

Figure 4. NeuroD1 does not induce microglia-to-neuron conversion even in TBI model.

(A) Experiment design. (B) Quantification of grip strength showing no improvement in NeuroD1-expressing TBI mice. Two-way ANOVA with multiple comparisons. (C) Quantification of rotarod performance showing no improvement in NeuroD1-expressing mice. Two-way ANOVA with multiple comparisons. (D) Representative confocal images of DAPI, GFP and NeuN co-staining results in NeuroD1^{MG} TBI mice, showing no co-localization of GFP with NeuN in either the lesion core or distal regions. Scale bar, 50 μm. (E) Quantification of the percentage of GFP^{+}NeuN^{+} cells among total NeuN^{+} cells in both the lesion area and distal area. n.d., not detected. (F) Representative confocal images of DAPI, GFP, and MAP2 in NeuroD1^{MG} mice, showing no co-localization of GFP with MAP2 in either the lesion core or distal regions. Scale bar, 50 μm. (G) Quantification of the percentage of GFP^{+}MAP2^{+} cells among total MAP2^{+} cells in the lesion area and distal region. n.d., not detected. (H) UMAP reduction shows the cell types of the FACS-sorted reporter^{+} cells in each group; note that there are no neurons. (I) Feature plot showing that the microglia-specific marker *P2ry12* was highly expressed even under TBI conditions, but the neuron-specific marker *Rbfox3* was barely expressed. (J) Violin plot showing the expression of microglia-specific genes (*Hexb* and *Tmem119*) and neuron-specific genes (*Tubb3* and *Map2*) in the collected cells.

To further investigate whether NeuroD1 expression could induce microglia-to-neuron conversion, we performed immunostaining on these brains. In both lesion core and distal regions, the GFP-labeled NeuroD1-expressing microglia did not co-localize with the neuronal marker NeuN (Figure 4D, E) and MAP2 (Figure 4F, G), similar to what was observed in control group (data not shown). Besides, we collected reporter (tdTomato or GFP) positive cells in both physiological and TBI condition for scRNA-seq, On the basis of cell type-specific annotations, we identified the cell types of the sorted cells and found no evidence of neuronal clusters in the scRNA-seq results (Figure 4H). Additionally, the microglial markers *P2ry12*, *Hexb*, and *Tmem119* remained highly expressed in reporter^{+} microglia (Figure 4I, J), whereas neuronal markers such as *Rbfox3*, *Tubb3*, and *Map2* were absent in both control and NeuroD1-overexpressing microglia (Figure 4I,J). Overall, these findings demonstrate that NeuroD1 fails to induce microglia-to-neuron conversion, even in the context of TBI.

Discussion

Our study provides compelling evidence that ectopic expression of NeuroD1 does not induce microglia-to-neuron conversion in the adult mouse brain. By employing virus-independent genetic lineage tracing and two-photon *in vivo* imaging, we systematically assessed the cell fate of NeuroD1-expressing microglia under both physiological and disease conditions. Across all approaches, NeuroD1-expressing microglia consistently retained their microglial identity and failed to acquire neuronal markers or morphology. These findings stand in contrast to previous reports claiming NeuroD1-mediated microglia-to-neuron conversion(25, 34), and instead support the notion that earlier observations may have resulted from experimental artifacts such as viral off-target expression(22, 26, 32, 35).

Previous studies have highlighted the challenges in validating direct glia-to-neuron reprogramming(26, 32). While initial reports demonstrated that the overexpression of single transcription factors such as SOX2, ASCL1, or NeuroD1 could convert glial cells into neurons, subsequent investigations using rigorous lineage tracing or live imaging failed to reproduce some of these inter-lineage conversions(21, 33). Our results reinforce these concerns by showing that even in a brain injury environment, NeuroD1 is insufficient to drive microglial fate conversion. In fact, our long-time observation revealed the disappearance of NeuroD1-expressing microglia over time, consistent with our prior finding that NeuroD1 overexpression induces BCL2-dependent apoptosis in microglia(32). Thus, rather than promoting neuronal reprogramming, NeuroD1 expression appears to compromise microglial survival. The combined evidence of LC3/P62 accumulation and increased TUNEL positivity, together with longitudinal in vivo imaging and prior in vitro data, indicates that NeuroD1 overexpression compromises microglial homeostasis and promotes cell death rather than inducing microglia-to-neuron conversion. This may also explain why the reporter efficiency of NeuroD1^{MG} is lower than that of Ai14^{MG} (quantification data not shown). These results suggest that NeuroD1 promotes microglial loss through multiple stress pathways rather than facilitating neuronal reprogramming.

Importantly, our data also demonstrate that NeuroD1 expression in microglia does not provide functional benefits in the TBI model. Behavioral assessments, including grip strength, and rotarod tests, revealed no improvement in motor function, which correlates with the absence of microglia-to-neuron conversion observed histologically. This discrepancy with previous claims that NeuroD1 promotes functional recovery following stroke or injury likely reflects differences in experimental design, particularly the reliance on viral delivery systems prone to off-target effects(34, 36). Our use of a virus-free genetic strategy ensures that NeuroD1 expression is restricted to microglia, thereby providing a more definitive evaluation of its reprogramming capacity. Although microglia may not represent a suitable cellular source for neuronal conversion, our team has developed an alternative therapeutic strategy based on microglia replacement(37, 38). Notably, this approach has been successfully translated into clinical practice and was shown to halt disease progression in patients with adult-onset leukoencephalopathy with axonal spheroids and pigmented glia (ALSP), supporting microglia as a promising target for cell-based therapies in neurological diseases(39).

Together, these findings underscore the necessity of applying stringent lineage-tracing approaches and multimodal validation strategies when evaluating cell fate conversion. While glia-to-neuron reprogramming remains a promising avenue for regenerative medicine, our results caution against premature translation of NeuroD1-based approaches into clinical settings. The lack of microglia-to-neuron conversion observed here does not diminish the therapeutic potential of targeting microglia in brain disorders; rather, it highlights the importance of exploring alternative strategies that preserve or modulate microglial functions without attempting to force lineage conversion. We agree the potential that NeuroD1 is able to induce stem cells or stem-like cells conversion(40), but direct microglia-to-neuron conversion is not applicable. Future studies should focus on identifying context-dependent mechanisms that may enable or restrict glial plasticity, and on developing approaches that combine genetic, epigenetic, and environmental cues to achieve reliable and functional neuronal reprogramming.

Materials and Methods

Animals

Cx3cr1-CreER[B6.129P2(C)-Cx3cr1$^{tm2.1(cre/ERT2)Jung}$/J, Stock No: 020940], Ai14 [B6.Cg-Gt(ROSA)26Sor$^{tm14(CAG-tdTomato)Hze}$/J, Stock No: 007914], LSL-Neurod1-GFP [Gt(ROSA)26Sor$^{tm1(Neurod1-EGFP)Able}$/BfriJ, Stock No: 034697] mice were purchased from The Jackson Laboratory. CX3CR1-CreER mice were crossed with LSL-Neurod1-EGFP mice to obtain Cx3cr1-CreER$^{+/-}$::LSL-Neurod1-EGFP$^{+/+}$ (NeuroD1^{MG}) mice. Similarly, Cx3cr1-CreER mice were crossed with Ai14 mice to obtain Cx3cr1-CreER::Ai14 (Ai14^{MG}) mice. All animals were housed in the Animal Facility of the Department of Laboratory Animal Science at Fudan University on a 12-h light−dark cycle with food and water provided ad libitum. No significant sex differences were observed in this study.

Drug administration

For the NeuroD1^{MG} and Ai14^{MG} mice, tamoxifen at 150 mg/kg body weight was administered via intragastric gavage (i.g.) for four consecutive days to induce loxP-dependent recombination.

Tissue preparation for immunohistochemistry

The animals were deeply anesthetized with 1% pentobarbital sodium (60 mg/kg) via intraperitoneal injection and transcranially perfused with cold 0.01 M PBS and cold 4% paraformaldehyde (PFA). The brains were immediately separated from the skulls and postfixed in 4% PFA for 24h at 4°C. For vibratome sectioning, brains were directly cut into coronal sections at the desired thickness using a Leica vibratome after post-fixation. For cryo-sectioning, brains were dehydrated in 30% sucrose in 0.01 M PBS at 4 °C for 2–3 days, followed by immersion in fresh 30% sucrose for an additional day. Tissue sections containing the regions of interest were then cut at 35 or 40 μm thickness using a Leica CM1950 cryostat.

Immunohistochemistry

The brain sections were rinsed 3 times in 0.01 M PBS for 10 min. The samples were blocked with 0.01 M PBS containing 0.3% Triton X-100 and 4% normal donkey serum (NDS, Jackson ImmunoResearch, Cat#: 017-000-121) at room temperature (RT) for 2 h. The samples were subsequently incubated with primary antibodies in 0.3% PBST containing 1% NDS at RT overnight. The samples were rinsed 3 times with 0.03% PBST for 10 min and then incubated with fluorescent dye-conjugated secondary antibodies in 0.03% PBST containing 1% NDS at RT for 2 h, together with 1:500 4’,6-diamidino-2-phenylindole (DAPI, Sigma−Aldrich, Cat#: D9542-10MG). Finally, the samples were rinsed with 0.03% PBST for 10 min 3 times, and the slides were mounted with antifade mounting medium. The edges of the cover glass were then sealed with nail enamel.

The primary antibodies used in this study were as follows: rabbit anti-Iba1 (Wako, Cat#: 019-19741, 1:500), goat anti-IBA1 (Abcam, Cat#: ab5076, 1:500), goat anti-GFP (Abcam, Cat#: AB6673, 1:500), goat anti-mCherry (Biorbyt, cat#: orb11618, 1:500), rabbit anti-GFP (Invitrogen, Cat#: A-11122,

1:1000), mouse anti-NEUN (Abcam, Cat#: ab104224, 1:500), rabbit anti-NeuroD1 (Abcam, Cat#: ab109224, 1:500), rabbit anti-RFP (Abcam, Cat#: ab62341, 1:1000), rabbit anti-DCX (Abcam, Cat#: ab18723, 1:200), mouse anti-MAP2 (Sigma, Cat#M9942: a, 1:2000), and rabbit anti-TUJ1 (Sigma, Cat#: T3952, 1:2000), mouse anti-LC3B (Cell Signaling Technology, Cat#: 83506T, 1:200); rabbit anti-p62 (Cell Signaling Technology, Cat#: 23214T, 1:500). The secondary antibodies used were as follows: AF488 donkey anti-goat IgG (Jackson ImmunoResearch, Cat#: 705-545-003, 1:2000), AF488 donkey anti-rabbit IgG (Jackson ImmunoResearch, Cat#: 711-545-152, 1:2000), AF568 donkey anti-rabbit IgG (Invitrogen by Thermo Fisher Scientific, Cat#: A10042, 1:2000), AF568 donkey anti-goat IgG (Invitrogen by Thermo Fisher Scientific, Cat#: A11057, 1:2000), AF647 donkey anti-rabbit IgG (Jackson ImmunoResearch, Cat#: 711-605-152, 1:2000), AF647 donkey anti-mouse IgG (Jackson ImmunoResearch, Cat#: 715-605-151, 1:2000), and AF647 donkey anti-goat IgG (Jackson ImmunoResearch, Cat#: 705-605-003, 1:2000).

In situ apoptosis assay

A commercial Tunnel Cell Apoptosis Detection Kit (Service bio, Cat#: G1502-50T; Elab science, Cat#: E-CK-A321) was used to detect in situ cell apoptosis. Briefly, brain sections were treated with Proteinase K (20 ug/mL) for 10 mins at RT. Then, brain sections were incubated with equilibration buffer for 10 minutes at RT. Next, apoptotic cells were labeled by TMR-5-dUTP or FITC-dUTP labeling mix at RT and counterstained with DAPI. Positive controls were treated with DNase I and negative controls were labeled by buffer without recombinant TdT enzyme.

Confocal microscopy

Confocal images of the fluorescent samples were acquired via 20x (NA 0.75), 40x (NA 1.30) or 60x (NA 1.40) objectives of a Nikon A2 confocal microscope. The Z-stacked focal planes were taken and maximally projected by ImageJ, whereas brightness and contrast were adjusted in ImageJ if necessary.

Tile scans of whole coronal brain sections were captured with an Olympus VS120 or VS200 system and exported from OlyVIA Software in TIFF format. Further data analysis was carried out in ImageJ.

Two-photon surgery and imaging

Two-photon cranial window surgery was performed on mice anesthetized with isoflurane (3% induction, 1.2%-1.5% maintenance). A 3.5 mm-diameter circular cranial window was created at the skull above the sensory cortex, and a same-diameter circular D263T glass slice was implanted. The cranial window and a head bar were bonded using glue and dental cement to maintain stability. In addition to performing routine postoperative care, the mice were injected intraperitoneally with antibiotics and anti-inflammatory drugs (dexamethasone sodium phosphate injection and ceftiofur sodium for injection) for five consecutive days.

Two-photon imaging was performed on days 18, 22, 26, and 30 post-tamoxifen induction (as shown in the timeline in Fig. 2). During imaging, the mice were anesthetized with isoflurane (3% induction, 1.2%-1.5% maintenance), and body temperature was maintained by a heating pad. Imaging was performed via a self-developed two-photon microscopy system (developed by the Institute for Translational Brain Research, Fudan University) with one resonant and one galvo scan mirror. The excitation was delivered with a Coherent Chameleon Ti-Sapphire pulsed laser. The fluorescence emission was filtered with a Semrork FF01-520/35-25, FF01-593/46 filter and detected with a Hamamatsu photomultiplier tube (H7422-40P). The EGFP signal in Cx3cr1-CreER::LSL-Neurod1-EGFP mice was excited by a 920 nm laser and imaged via a 16x, 0.8 NA water-dipping objective (Nikon). Images were acquired at a depth of approximately 100 μm below the dura using ScanImage(41) at step intervals of 2 μm. Each Z-axis plane image (512×512 pixels) was imaged at a consistent zoom factor (~300 × 300 μm area) and acquired at a 1.06 Hz frame rate.

Image processing was performed via ImageJ, and the Z-stack image containing the target cells was selected. Brightness and contrast were adjusted if needed, and the maximal projection was performed. Video processing was performed via Adobe Premiere software.

AAV vectors, lentivirus preparation, and stereotaxic injection

The AAV vectors were purchased from Obio Technology, Ltd., and PackGene Biotech, Inc., and were as follows: *AAV1/2-CMV-EGFP*, *AAV5/2-CMV-EGFP*, *AAV6/2-CMV-EGFP*, *AAV8/2-CMV-EGFP*, *AAV9/2-CMV-EGFP*, *AAV2-DJ-CMV-EGFP*, *AAV2-retro-CMV-EGFP*, *AAV-PHP.eB-CMV-EGFP*, *AAV6-CX3CR1-GFP*, *AAV8-CX3CR1-GFP*, *AAV9-CX3CR1-GFP*, *AAV6-CD68-GFP*, *AAV8-CD68-GFP*, and *AAV9-CD68-GFP*.

All lentiviruses were packaged by Obio Technology, Ltd., according to the author's design and requirements. All lentiviruses were packaged in HEK293 cells, and the packaged plasmids consisted of pMDL, VSV-G and pREV. The following lentiviral vectors were used: *pLenti-CAG-flag-NeuorD*1, *pLenti-CAG-flag-MCS*, *pLenti-CMV-GFP*, *pLenti-CX3CR1-GFP* and *pLenti-CD68-GFP*.

For intracranial injection, the mouse was anesthetized with isoflurane. The stereotaxic injection coordinates were +1.0 mm anterior/posterior, ± 1.7 mm medial/lateral, and −0.75 mm dorsal/ventral.

Traumatic brain injury (TBI)

TBI was induced using the controlled cortical impact (CCI) model as previously described(42). Briefly, mice were anesthetized with ketamine (100 mg/kg) and xylazine (10 mg/kg) and placed in a stereotaxic frame (Stoelting, Wood Dale, IL, USA). Body temperature was maintained at 37.0 ± 0.5 °C using a heating pad throughout the procedure. After scalp disinfection, a midline incision (1.5–2 cm) was made to expose the skull. A 4 mm craniotomy was performed over the right parietal cortex (between bregma and lambda, 1 mm lateral to the midline) using a portable drill, taking care to preserve the dura mater. Mice with damaged dura were excluded from further analysis. Cortical impact was delivered using a 3 mm rounded steel impactor (PinPoint PCI3000, Hatteras Instruments Inc., USA) at a velocity of 1.5 m/s, impact depth of 1.5 mm, and dwell time of 100 ms. After impact, the bone flap was sealed with sterile bone wax and the scalp was sutured. Sham-operated mice underwent the same surgical procedures without cortical impact. Following surgery, mice were placed in a 37 °C recovery chamber until fully ambulatory.

Rotarod test

The mice were acclimated in the behavioral room for half an hour before testing. Briefly, during the training phase, the mice were trained to walk on a rotating rod at 5 RPM, allowing them to maintain balance by walking forward. Each mouse was placed on the rod for 60 seconds, after which it was returned to its home cage. This procedure was repeated 3 times with a 10-min interval. In the testing phase, the mice were placed in separate lanes on the rod, which was set to accelerate from 4 to 40 RPM over a 300-second period. This procedure was repeated three times at approximately 30-min intervals. The latency to fall was recorded for statistical analysis.

Grip strength test

The mice were housed in the behavioral room half an hour before the behavioral testing. Briefly, the grip strength meter was positioned on the table. Each mouse was gently held by the tail and placed with all the paws on the grip strength grid. The mouse was then gently pulled back until its grasp was released, after which the maximum holding force was recorded. This procedure was repeated 6 times, and the maximum force was used for statistical analysis.

Single-cell preparation and fluorescence-activated cell sorting (FACS)

For scRNA-seq, FACS was used to harvest GFP^+ or $tdTomato^+$ cells from tamoxifen-treated *Cx3cr1-creER*::*LSL-Neurod1-GFP* and *Cx3cr1-CreER*::*Ai14* mice. Briefly, brains were dissected and cut into 1-mm^3 pieces using a mouse stainless steel brain matrix (RWD). The tissue pieces were digested in

3 ml of DMEM containing 8 U/ml papain (Sangon Biotech, cat: A501612), 125 U/ml DNase I (Sangon Biotech, cat: A510099), and 1.5 mg/ml trypsin inhibitor (Aladdin, cat: A274384) via a gentleMACS Octo Dissociator (Miltenyi) with the 37C_ABDK program.

After 30 min of digestion, the mixture was gently pipetted up and down and then filtered through a 70 μm cell strainer. The dissociated cells were centrifuged at 370 × g at RT for 10 min, and the supernatant was discarded. The cell pellets were resuspended in 4 ml of 30% Percoll (Cytiva, cat: 17089101) and centrifuged again at 370 × g and 17°C for 10 min to remove debris. After centrifugation, the supernatant was discarded, and the cells were washed once with DPBS containing 0.5% BSA. Before the cells were loaded onto the SONY MA900, they were stained with 7-AAD (BD Pharmingen, cat: 559925, 1:700) to label dead cells. Finally, the tdTomato^{+} 7-AAD^{-} or GFP^{+}7-AAD^{-} cells were collected for scRNA-seq immediately.

scRNA-seq data analysis

scRNA-seq was conducted via the MobiCube High-throughput Single Cell 3' Transcriptome Set V2.1 (PN-S050200301) and the MobiNova-100 microfluidic platform. The single-cell suspension was adjusted to a concentration of 700–1200 cells/μl and immediately loaded onto a chip for microdroplet formation via the MobiNova-100 system. Reverse transcription, cDNA amplification, and DNA library construction were carried out according to the manufacturer's protocol. High-throughput sequencing was performed in PE-150 mode.

FASTQ files were processed and aligned to the mouse reference genome (mm10) via MobiVision version 3.2, with unique molecular identifier (UMI) counts aggregated for each barcode. The resulting UMI count matrix was analyzed in R version 4.2.2 via Seurat version 4.3.0. To ensure data quality, we excluded low-quality cells and potential multiplets on the basis of the following criteria: cells with fewer than 200 genes or more than 5000 genes and cells with more than 10% UMIs mapped to mitochondrial genes. scRNA-seq data from the four groups were integrated via *IntegratedData* functions according to the manufacturer's instructions. The remaining data were normalized via the *NormalizeData* function and scaled with *ScaleData*. For scRNA-seq analysis, principal component analysis (PCA) was conducted on variable features, with the top 30 principal components (PCs) selected for clustering and visualization via tSNE and uniform manifold approximation and projection (UMAP). Cell clustering was performed with a resolution of 1 to annotate the cell types. Differentially expressed genes (DEGs) among cell groups were identified via the *FindMarkers* function with parameters set to min.pct = 0.1 and a log fold change (FC) threshold of 0.25 (Wilcoxon rank-sum test). Genes with $|\log2FC| > 0.25$ and $P < 0.05$ were considered significant DEGs and subsequently used for Gene Ontology (GO) analysis. Visualization of the results was performed via the *VlnPlot* and *FeaturePlot* functions.

Statistical analysis

Statistical analyses were performed with Prism 8.4.0 (GraphPad). Each data point represents the average statistical result of more than three brain sections in different bregma regions of one mouse. The results were evaluated independently in a double-blind manner. All the results are presented as the means ± standard deviations (SDs). One-way analysis of variance (ANOVA) with Holm−Sidak's multiple comparisons test (post hoc) was performed for multiple comparisons, whereas a two-tailed independent t test was used to compare the differences between two groups. No outliers were excluded.

Supporting Information

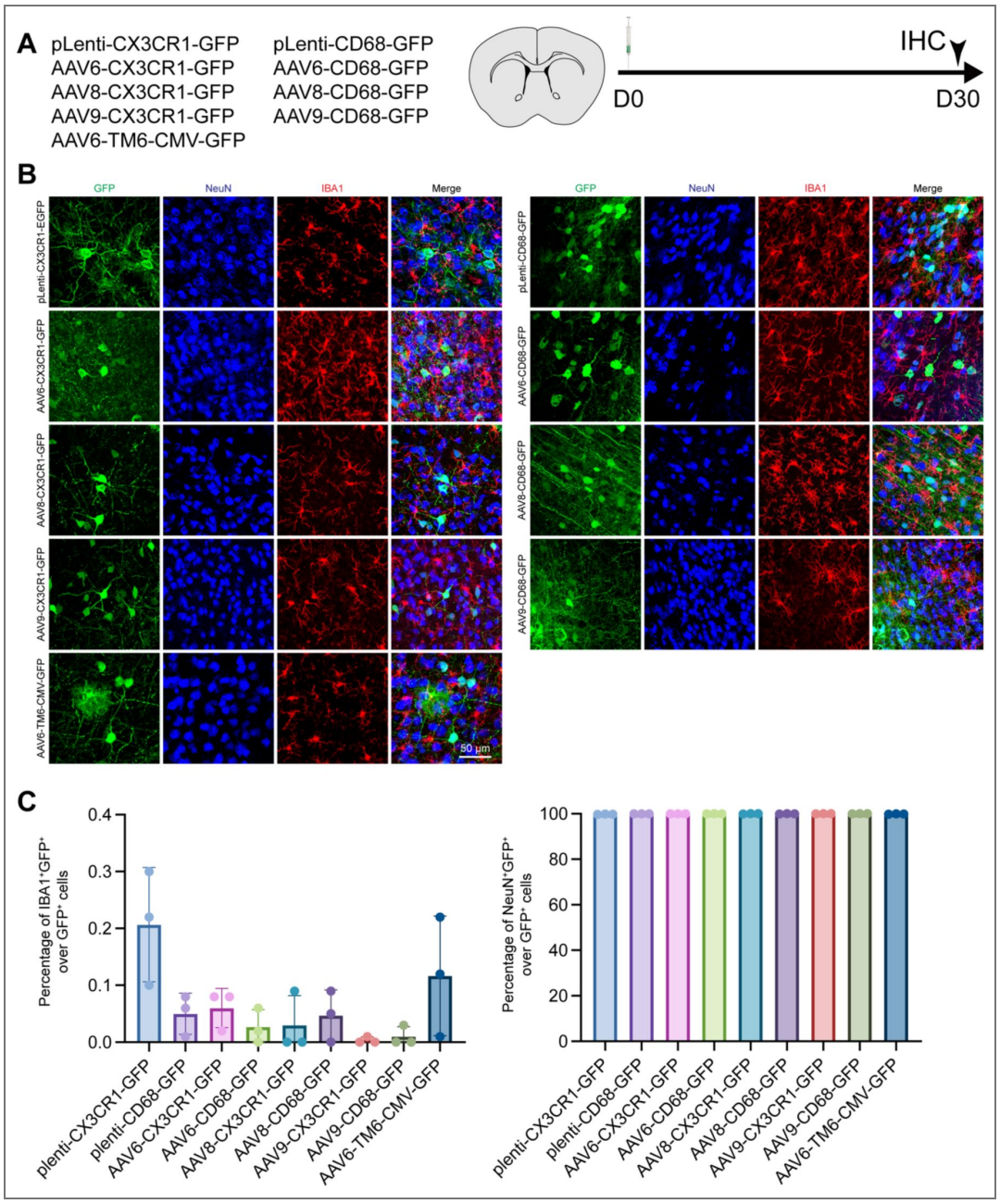

Fig. S1. Lentivirus- or AAV-based infection caused leaky neuronal expression *in vivo*. (**A**) The study design shows the different viruses used here. (**B**) Representative confocal images showing the expression of GFP, IBA1 and NEUN in the brains of the lentivirus- or AAV-infected mice. (**C**) The efficacy of infection was quantified, and the data are presented as the ratio of $IBA1^+GFP^+/GFP^+$ cells. N = 3 mice for each group.

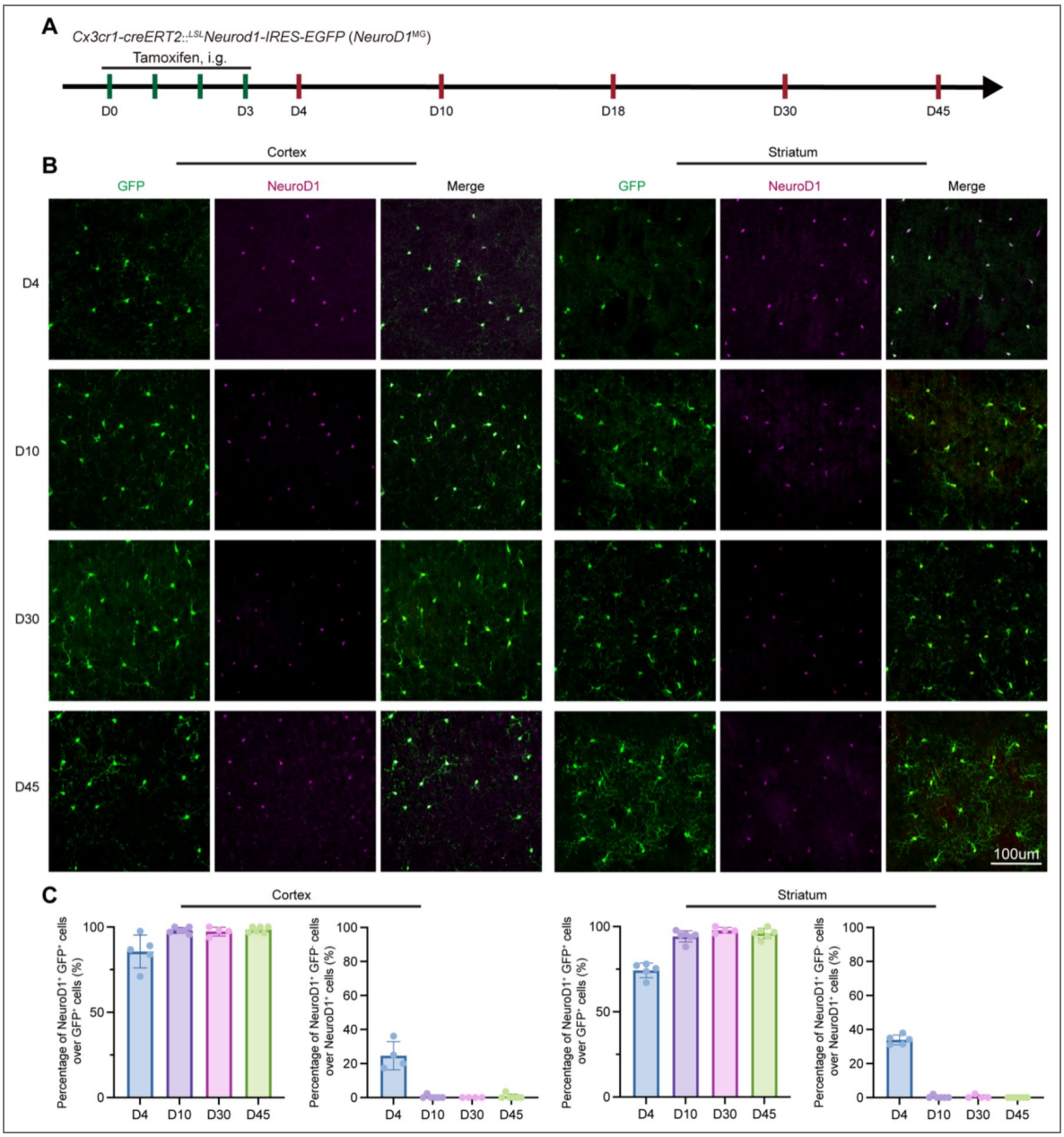

Fig. S2. NeuroD1 is robustly co-expressed in GFP-positive cells after Cre recombination.

(A) Experimental timeline. (B) Representative confocal images at D4, D10, D30 and D45 showing that NeuroD1 is robustly co-expressed in GFP-positive cells after Cre recombination. (C) Quantification of NeuroD1^{+}GFP^{+} double-positive cells in GFP^{+} cells and NeuroD1^{+}GFP^{-} in NeuroD1^{+} cells at D4, D10, D30 and D45. N = 5 mice for each group.

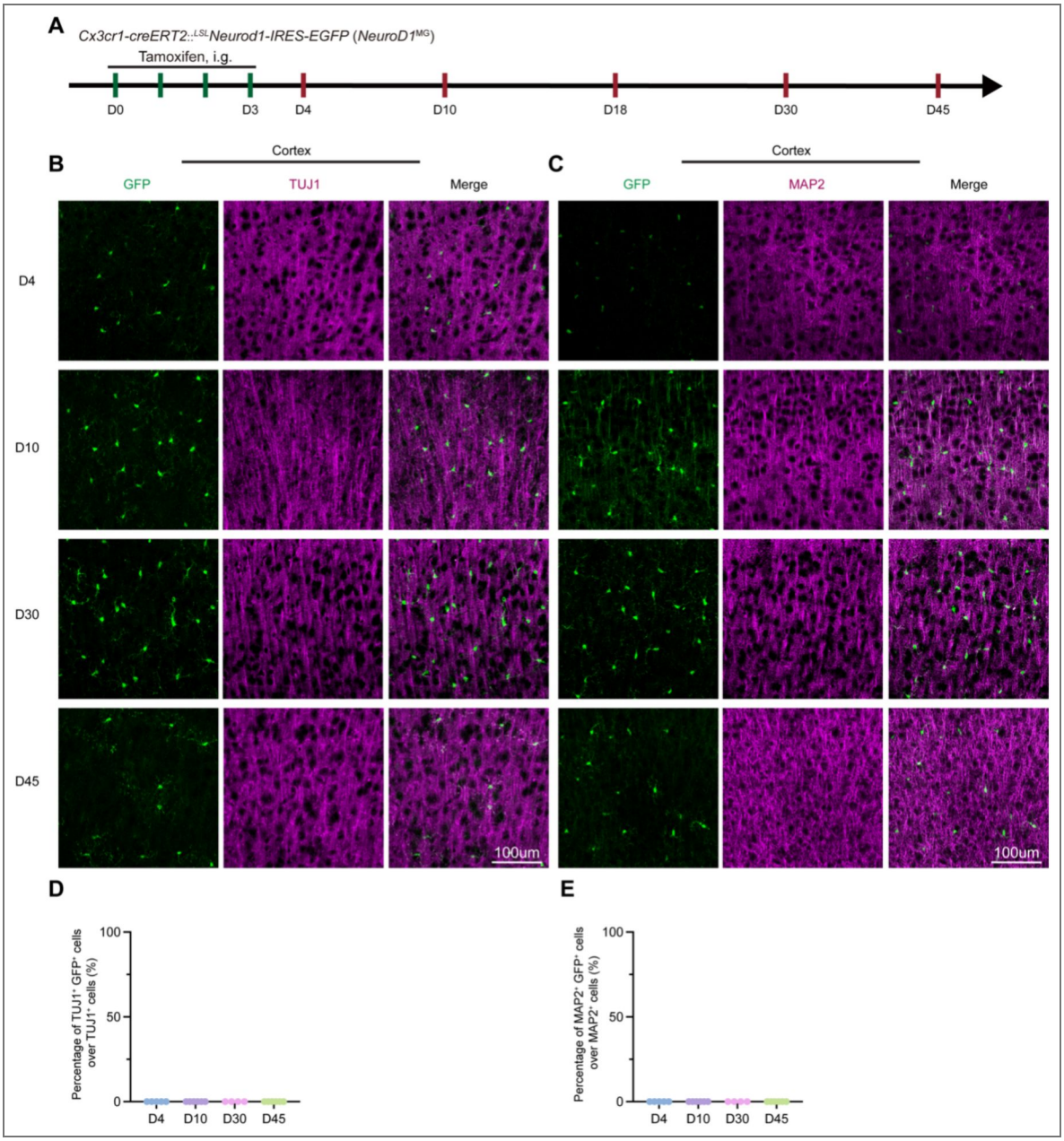

Fig. S3. Ectopic NeuroD1 expression in microglia does not induce microglia-to-neuron conversion, as GFP does not co-localize with TUJ1 and MAP2.

(A) Experimental timeline. (B) Representative confocal images at D4, D10, D30 and D45 showing that GFP is not co-labeled with TUJ1 in the brain. (C) Representative confocal images at D4, D10, D30 and D45 showing that GFP is not co-labeled with MAP2 in the brain. (D) Quantification of $TUJ1^{+}GFP^{+}$ double-positive cells among $TUJ1^{+}$ cells at D4, D10, D30 and D45. N = 4 or 5 mice for each group. (E) Quantification of $MAP2^{+}GFP^{+}$ double-positive cells among $MAP2^{+}$ cells at D4, D10, D30 and D45. N = 4 or 5 mice for each group.

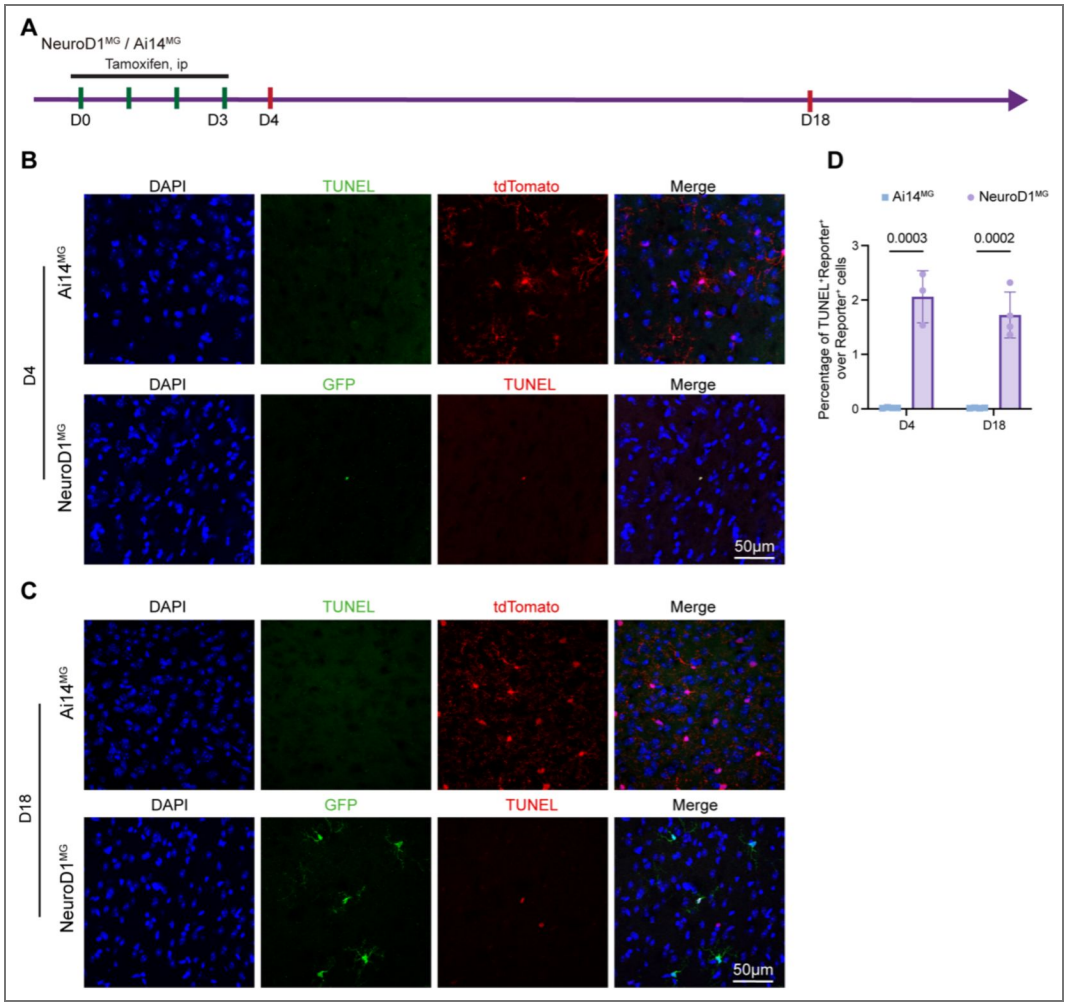

Fig. S4. TUNEL staining shows NeuroD1expression triggers microglia apoptosis.

(A) Experiment timeline. (B) Represent confocal image shows TUNEL^{+}reporter^{+} cells are observed in NeuroD1^{MG} mice at D4. Scale bar = 50μm. (C) Represent confocal image shows TUNEL^{+}reporter^{+} cells are observed in NeuroD1^{MG} mice at D18. Scale bar = 50μm. (D) Quantification result shows TUNEL^{+}reporter^{+} cells are higher than control group.

Data availability

The sequencing data generated in this study have been deposited in the Gene Expression Omnibus under accession number GSE277222. All other data supporting the findings of this study are available from the corresponding author upon reasonable request.

Acknowledgements

This work was supported by Brain Science and Brain-like Intelligence Technology–National Science and Technology Major Project (2022ZD0207200, 2022ZD0204700); National Natural Science Foundation of China (32571128, 323B2030, 325B2039); the Fellowship of China National Postdoctoral Program for Innovative Talents (BX20250132); the Fellowship of China Postdoctoral Science Foundation (2025M782569); Shanghai Pilot Program for Basic Research (21TQ014), Changping Laboratory (2025B-07-18) and Lin Gang Laboratory (LGL-8998-02). In addition, authors also express their gratitude and respect to all animals sacrificed in this study. During the preparation of this manuscript, the authors, as the non-native English speakers, used ChatGPT 4o and 5 to improve the language and enhance its readability.

Additional files

Video 1. This video shows that GFP$^+$ cells did not convert to neurons in vivo via 2-photon imaging at 18, 22, 26 and 30 days post-tamoxifen administration. Refers to Figure 3.

Additional information

Funding

Funder	Grant reference number	Author
MOST | National Natural Science Foundation of China (NSFC)	32571128	Bo Peng
MOST | National Natural Science Foundation of China (NSFC)	323B2030	Xiaoyu Li
MOST | National Natural Science Foundation of China (NSFC)	325B2039	Yanxia Rao
China Postdoctoral Science Foundation	2025M782569	Xiaoyu Li
China Postdoctoral Science Foundation	BX20250132	Xiaoyu Li
Shanghai Pilot Program for Basic Research	21TQ014	Bo Peng
Brain Science and Brain-like Intelligence Technology-National Science and Technology Major Project	2022ZD0207200	Bo Peng
Brain Science and Brain-like Intelligence Technology-National Science and Technology Major Project	2022ZD0204700	Yanxia Rao

Author ORCID iDs

Bo Peng: https://orcid.org/0000-0003-4183-5939

Author notes

Xiaoyu Li, Yuxin Li, Yue Cao: These authors contributed equally.

Author Contributions: B.P. and Y.R. conceived and designed this study. B.P. and Y.R. supervised and conceptualized this study. Y.R., B.P. and X.L. wrote the manuscript. X.L., Y.L., Y.C., N.H., P.O., Y.J., and S.G. performed most experiments. X.L. performed data analysis. All authors discussed the results and commented on this manuscript.

Competing interests: No competing interests declared

References

1. **Varvel NH,** et al. (2012) Microglial repopulation model reveals a robust homeostatic process for replacing CNS myeloid cells. *Proc Natl Acad Sci U S A* **109**:18150-18155 https://doi.org/10.1073/pnas.1210150109 | PubMed
2. **Huang Y,** et al. (2018) Repopulated microglia are solely derived from the proliferation of residual microglia after acute depletion. *Nature neuroscience* **21**:530-540 https://doi.org/10.1038/s41593-018-0090-8 | PubMed
3. **Li X,** et al. (2023) Transcriptional and epigenetic decoding of the microglial aging process. *Nat Aging* 1288-1311 https://doi.org/10.1038/s43587-023-00479-x | PubMed
4. **Guo Z,** et al. (2014) In vivo direct reprogramming of reactive glial cells into functional neurons after brain injury and in an Alzheimer's disease model. *Cell stem cell* **14**:188-202 https://doi.org/10.1016/j.stem.2013.12.001 | PubMed
5. **Heins N,** et al. (2002) Glial cells generate neurons: the role of the transcription factor Pax6. *Nature neuroscience* **5**:308-315 https://doi.org/10.1038/nn828 | PubMed
6. **Tai W,** et al. (2021) In vivo reprogramming of NG2 glia enables adult neurogenesis and functional recovery following spinal cord injury. *Cell Stem Cell* **28**:923-937.e924 https://doi.org/10.1016/j.stem.2021.02.009 | PubMed
7. **Niu W,** et al. (2013) In vivo reprogramming of astrocytes to neuroblasts in the adult brain. *Nature Cell Biology* **15**:1164-1175 https://doi.org/10.1038/ncb2843 | PubMed
8. **Niu W,** et al. (2013) In vivo reprogramming of astrocytes to neuroblasts in the adult brain. *Nat Cell Biol* **15**:1164-1175 https://doi.org/10.1038/ncb2843 | PubMed
9. **Niu W,** et al. (2015) SOX2 reprograms resident astrocytes into neural progenitors in the adult brain. *Stem Cell Reports* **4**:780-794 https://doi.org/10.1016/j.stemcr.2015.03.006 | PubMed
10. **Chanda S,** et al. (2014) Generation of induced neuronal cells by the single reprogramming factor ASCL1. *Stem Cell Reports* **3**:282-296 https://doi.org/10.1016/j.stemcr.2014.05.020 | PubMed
11. **Qian H,** et al. (2020) Reversing a model of Parkinson's disease with in situ converted nigral neurons. *Nature* **582**:550-556 https://doi.org/10.1038/s41586-020-2388-4 | PubMed
12. **Zhou H,** et al. (2020) Glia-to-Neuron Conversion by CRISPR-CasRx Alleviates Symptoms of Neurological Disease in Mice. *Cell* https://doi.org/10.1016/j.cell.2020.03.024 | PubMed
13. **Rao Y,** et al. (2021) NeuroD1 induces microglial apoptosis and cannot induce microglia-to-neuron cross-lineage reprogramming. *Neuron* **109**:4094-4108.e4095 https://doi.org/10.1016/j.neuron.2021.11.008 | PubMed
14. **Svendsen CN,** Sofroniew MV (2022) Lineage tracing: The gold standard to claim direct reprogramming in vivo. *Mol Ther* **30**:988-989 https://doi.org/10.1016/j.ymthe.2022.01.029 | PubMed
15. **Hoang T,** et al. (2023) Ptbp1 deletion does not induce astrocyte-to-neuron conversion. *Nature* **618**:E1-E7 https://doi.org/10.1038/s41586-023-06066-9 | PubMed
16. **Yang G,** et al. (2023) Ptbp1 knockdown failed to induce astrocytes to neurons in vivo. *Gene Ther* **30**:801-806 https://doi.org/10.1038/s41434-023-00382-5 | PubMed
17. **Xie Y,** Zhou J, Chen B (2022) Critical examination of Ptbp1-mediated glia-to-neuron conversion in the mouse retina. *Cell reports* **39**:110960 https://doi.org/10.1016/j.celrep.2022.110960 | PubMed
18. **Guo T,** et al. (2022) Downregulating PTBP1 fails to convert astrocytes into hippocampal neurons and to alleviate symptoms in Alzheimer's mouse models. *J Neurosci* https://doi.org/10.1523/jneurosci.1060-22.2022 | PubMed
19. **Hoang T,** et al. (2022) Genetic loss of function of Ptbp1 does not induce glia-to-neuron conversion in retina. *Cell reports* **39** https://doi.org/10.1016/j.celrep.2022.110849 | PubMed

20. **Chen W,** Zheng Q, Huang Q, Ma S, Li M (2022) Repressing PTBP1 fails to convert reactive astrocytes to dopaminergic neurons in a 6-hydroxydopamine mouse model of Parkinson's disease. *eLife* **11**:e75636 https://doi.org/10.7554/eLife.75636 | PubMed

21. **Xie Y,** Zhou J, Wang LL, Zhang CL, Chen B (2023) New AAV tools fail to detect Neurod1-mediated neuronal conversion of Muller glia and astrocytes in vivo. *EBioMedicine* **90**:104531 https://doi.org/10.1016/j.ebiom.2023.104531 | PubMed

22. **Leib D,** Chen YH, Monteys AM, Davidson BL (2022) Limited astrocyte-to-neuron conversion in the mouse brain using NeuroD1 overexpression. *Mol Ther* **30**:982-986 https://doi.org/10.1016/j.ymthe.2022.01.028 | PubMed

23. **Wang LL,** et al. (2021) Revisiting astrocyte to neuron conversion with lineage tracing in vivo. *Cell* **184**:5465-5481 e5416 https://doi.org/10.1016/j.cell.2021.09.005 | PubMed

24. **Matsuda T,** et al. (2019) Pioneer Factor NeuroD1 Rearranges Transcriptional and Epigenetic Profiles to Execute Microglia-Neuron Conversion. *Neuron* **101**:472-485 e477 https://doi.org/10.1016/j.neuron.2018.12.010 | PubMed

25. **Matsuda T,** Nakashima K (2021) Clarifying the ability of NeuroD1 to convert mouse microglia into neurons. *Neuron* https://doi.org/10.1016/j.neuron.2021.11.012 | PubMed

26. **Rao Y,** Peng B (2022) Failure of observing NeuroD1-induced microglia-to-neuron conversion in vitro is not attributed to the low NeuroD1 expression level. *Mol Brain* **15** https://doi.org/10.1186/s13041-022-00912-z | PubMed

27. **Irie T,** et al. (2023) Direct neuronal conversion of microglia/macrophages reinstates neurological function after stroke. *Proceedings of the National Academy of Sciences* **120**:e2307972120 https://doi.org/10.1073/pnas.2307972120 | PubMed

28. **Rao Y,** et al. (2021) NeuroD1 induces microglial apoptosis and cannot induce microglia-to-neuron cross-lineage reprogramming. *Neuron* **109**:4094-4108.e4095 https://doi.org/10.1016/j.neuron.2021.11.008 | PubMed

29. **Rosario AM,** et al. (2016) Microglia-specific targeting by novel capsid-modified AAV6 vectors. *Mol Ther Methods Clin Dev* **3**:16026 https://doi.org/10.1038/mtm.2016.26 | PubMed

30. **Yona S,** et al. (2013) Fate mapping reveals origins and dynamics of monocytes and tissue macrophages under homeostasis. *Immunity* **38**:79-91 https://doi.org/10.1016/j.immuni.2012.12.001 | PubMed

31. **Li HJ,** et al. (2019) Intestinal Neurod1 expression impairs paneth cell differentiation and promotes enteroendocrine lineage specification. *Scientific reports* **9**:19489 https://doi.org/10.1038/s41598-019-55292-7 | PubMed

32. **Rao Y,** et al. (2021) NeuroD1 induces microglial apoptosis and cannot induce microglia-to-neuron cross-lineage reprogramming. *Neuron* **109**:4094-4108 e4095 https://doi.org/10.1016/j.neuron.2021.11.008 | PubMed

33. **Heinrich C,** et al. (2014) Sox2-mediated conversion of NG2 glia into induced neurons in the injured adult cerebral cortex. *Stem Cell Reports* **3**:1000-1014 https://doi.org/10.1016/j.stemcr.2014.10.007 | PubMed

34. **Irie T,** et al. (2023) Direct neuronal conversion of microglia/macrophages reinstates neurological function after stroke. *Proc Natl Acad Sci U S A* **120**:e2307972120 https://doi.org/10.1073/pnas.2307972120 | PubMed

35. **Wang LL,** et al. (2021) Revisiting astrocyte to neuron conversion with lineage tracing in vivo. *Cell* **184**:5465-5481.e5416 https://doi.org/10.1016/j.cell.2021.09.005 | PubMed

36. **Matsuda T,** et al. (2019) Pioneer Factor NeuroD1 Rearranges Transcriptional and Epigenetic Profiles to Execute Microglia-Neuron Conversion. *Neuron* **101**:472-485.e477 https://doi.org/10.1016/j.neuron.2018.12.010 | PubMed

37. **Rao Y,** Bai Y, Li X, Du B, Peng B (2025) The evolution of microglia replacement: A new paradigm for CNS disease therapy. *Cell Stem Cell* **32**:1807-1832 https://doi.org/10.1016/j.stem.2025.10.014 | PubMed

38. **Xu Z,** et al. (2020) Efficient Strategies for Microglia Replacement in the Central Nervous System. *Cell Rep* **32**:108041 https://doi.org/10.1016/j.celrep.2020.108041 | PubMed

39. **Wu J,** et al. (2025) Microglia replacement halts the progression of microgliopathy in mice and humans. *Science* **389**:eadr1015 https://doi.org/10.1126/science.adr1015 | PubMed

40. **Saito Y,** et al. (2025) NEUROD1 efficiently converts peripheral blood cells into neurons with partial reprogramming by pluripotency factors. *Proc Natl Acad Sci U S A* **122**:e2401387122 https://doi.org/10.1073/pnas.2401387122 | PubMed

41. **Pologruto TA,** Sabatini BL, Svoboda K (2003) ScanImage: Flexible software for operating laser scanning microscopes. *BioMedical Engineering OnLine* **2** https://doi.org/10.1186/1475-925x-2-13 | PubMed

42. **Cai L,** et al. (2025) ALKBH5 demethylates the m(6)A modification of SOCS3 in microglia/macrophages and alleviates neuroinflammation after brain injury. *Proc Natl Acad Sci U S A* **122**:e2504697122 https://doi.org/10.1073/pnas.2504697122 | PubMed

Xiaoyu Li, Yanxia Rao, Bo Peng (2024) scRNA-seq data from normal microglia and NeuroD1-overexpressing microglia under both normal and TBI conditions. NCBI Gene Expression Omnibus. ID GSE277222 https://www.ncbi.nlm.nih.gov/geo/query/acc.cgi?acc=GSE277222

Peer reviews

Reviewer #1 (Public review):

Summary:

This study revisits an important and controversial question in brain repair: whether NeuroD1 can convert brain immune cells into nerve cells in vivo. Using a virus-free genetic system, in vivo imaging, injury experiments, and single-cell profiling, the authors provide convincing evidence that NeuroD1-expressing cells do not become nerve cells under the tested conditions. Instead, these cells largely retain their original immune-cell identity, and some appear to undergo cellular stress or loss.

Strengths:

The main strength of the work is that it tests this question with a cleaner genetic strategy, avoiding some of the concerns associated with viral delivery and unintended cell labeling. Although the overall conclusion is consistent with the authors' previous work, the current study adds useful independent evidence, particularly through the virus-free fate-mapping system and live imaging in the brain.

Weaknesses:

There are some limitations. In the injury experiment, the labeled cells may include both resident brain immune cells and blood-derived immune cells recruited after injury, so the authors should be cautious when referring to all labeled cells as microglia. The level of NeuroD1 expression achieved by the genetic system is also not fully defined, which matters because the effects of such a cell-fate regulator may depend on expression level. Finally, the tested time window may not fully address very delayed or incomplete neuronal differentiation.

Overall, this is a useful and careful study that supports the conclusion that NeuroD1 does not drive brain immune cells to become nerve cells in the tested settings. It should be valuable for researchers studying brain repair, cell fate conversion, and genetic fate mapping, and it

provides a clear caution against overinterpreting reprogramming results based only on viral labeling.

https://doi.org/10.7554/eLife.112083.1.sa1

Reviewer #2 (Public review):

Summary:

In vivo glia-to-neuron conversion emerges as a potential regeneration-based therapeutic strategy for neural injuries and diseases. However, controversies exist in this exciting field, largely arising from the non-stringent methods employed for analyzing in vivo neuronal conversions. The study by Li et al. directly addressed this controversy regarding Neurod1-mediated microglia-to-neuron conversion. They took advantage of two transgenic mouse lines to specifically express Neurod1 in the microglia of adult mouse brains. Results from immunohistochemistry, in vivo live-cell imaging, and scRNA-seq convincingly demonstrate that microglia cannot be converted in vivo to neurons by ectopic Neurod1 expression under both normal and injury conditions. Instead, it induces microglia death, consistent with their earlier findings. These solid results, though negative, are critical additions to the field and further support that stringent lineage tracing methods are essential for studying in vivo cell reprogramming. Overall, the studies are rigorously designed and executed. Only minor issues need to be dealt with.

https://doi.org/10.7554/eLife.112083.1.sa0